

Promising photovoltaic efficiency of a layered silicon oxide crystal Si₃O

Sejoong Kim,^{1,2} Kisung Chae,^{2,3,4,*} and Young-Woo Son^{2,†}

¹University of Science and Technology (UST), Daejeon 34113, Korea

²Korea Institute for Advanced Study, Seoul 02455, Korea

³Department of Chemistry and Biochemistry, University of California, San Diego, La Jolla, CA 92093, United States

⁴Materials Science and Engineering Department, The University of Texas at Dallas, Richardson, Texas 75080, United States

(Dated: August 7, 2020)

Computational searching and screening of new functional materials exploiting earth abundant elements can accelerate developments of their energy applications. Based on a state-of-the-art materials search algorithm and *ab initio* calculations, we demonstrate a recently suggested stable silicon oxide with a layered structure (Si₃O) as an ideal photovoltaic material. With many-body first-principles approaches, the monolayer and layered bulk of Si₃O show direct quasiparticle gaps of 1.85 eV and 1.25 eV, respectively, while an optical gap of about 1.2 eV is nearly independent of the number of layers. Spectroscopic limited maximum efficiency (SLME) is estimated to be 27% for a thickness of 0.5 μm , making it a promising candidate for solar energy applications.

Discovery of efficient, reliable and safe photovoltaic (PV) materials will be a critical booster to realize a sustainable energy alternative with solar cells [1]. Among various potential candidates for the next generation solar cells, two-dimensional (2D) materials have gained significant attention for their few-atom thickness, exceptional stability and diverse electronic structures tunable by the number of layers and heterostructure formations [2–7]. To uncover their full potentials, it is important to search and test 2D materials candidates thoroughly [8, 9].

In discovering materials *in silico*, various computational materials design methods have been adopted to accelerate the discovery. Crystal structure predictions based on global optimization [10–12] have been used to predict novel materials with unusual properties [13–15]. Together with these impressive developments in materials predictions, recent progresses in the data-driven sciences such as text-mining and natural language processing for synthesis of inorganic materials [16] may further accelerate the computer-aided materials discovery. For 2D materials, high-throughput materials search algorithms [8, 9, 17, 18] have been used for screening the optimal material candidates for solar cell applications [17–21]. Considering current domination of silicon solar cells, however, a suitable 2D silicon material that is readily applicable for harvesting solar light is still lacking.

Recently, a family of novel 2D materials composed of group IV and VI elements, namely T₃X (T=C, Si, Ge, Sn; X=O, S, Se, Te), have been predicted, demonstrating various electronic properties ranging from band insulator to quantum spin Hall insulator [22]. Those novel 2D crystals have been found by using a new crystal structure prediction method: SANDWICH (Search by *Ab initio* Novel Design via Wyckoff positions Iteration in Conformational Hypersurface) [22, 23]. This method has a particular merit over the others in finding stable but unconventional 2D atomic structures with a low atomic density, e.g., hollow structures [22, 23]. Among the T₃X compounds, 2D Si₃O crystal shown in Fig. 1 has the convex-hull stability and a direct band gap, making it a good candidate for optoelectronic devices [22, 23].

In this work, we provide computational evidences showing

that Si₃O has noticeable merits for solar cell application. Our evaluation of the spectroscopic limited maximum efficiency (SLME) [17] of Si₃O reaches 26.8% for a thickness of 0.5 μm . As a good metric for screening PV materials [17], the SLME was also used as a key descriptor to test over a million materials in a machine-learning approach, searching for solar energy application [18]. The SLME value in this study is comparable to the best 2D candidates in the database of Ref. [18]. To obtain an accurate value, we perform fully converged many-body *ab initio* calculations on quasiparticle (QP) spectra and exciton binding energies of a monolayer and bulk, respectively. It is shown that the both have direct gaps, differing from other semiconducting 2D materials [24]. Considering other merits of Si₃O such as earth-abundant, non-toxic and simple elements, light weight, a superb stability [22] and a very light effective mass [23], we expect that the proposed layered silicon oxide will play an important role in silicon-based energy applications once it be synthesized. We briefly discuss synthesis and stability of the Si₃O in the Electronic Supplementary Information (ESI).

We use atomic structures of a monolayer and layered bulk of Si₃O obtained from our SANDWICH code, as shown in Figs. 1(b) and 1(c), respectively [22, 23]. We perform the mean-field [26] density functional theory (DFT-PBE) calculations using QUANTUM ESPRESSO [27, 28]. Grimme’s DFT-D2 method [29] is used for interlayer interactions. On top of the DFT-PBE calculations, the G_0W_0 [30, 31] and Bethe-Salpeter equation (BSE) [32–37] calculations are performed by using BERKELEYGW [38]. The Coulomb interaction truncation [39] is used to simulate the isolated monolayer. Due to a slow convergence of the QP energies in 2D systems [40], we carefully converge the QP energy gap within 50 meV by varying vacuum size, k -point grid, energy cutoff for dielectric matrix and the number of unoccupied bands. We also calculate self-consistent Green’s function to obtain QP gaps, i.e., GW_0 approximation. It is known that the band gaps obtained by the GW_0 method converge to the QP gap linearly interpolated from the G_0W_0 gap [35]. After three iterations, the difference between them becomes smaller than 5 meV. Further details of calculations can be found in the ESI.

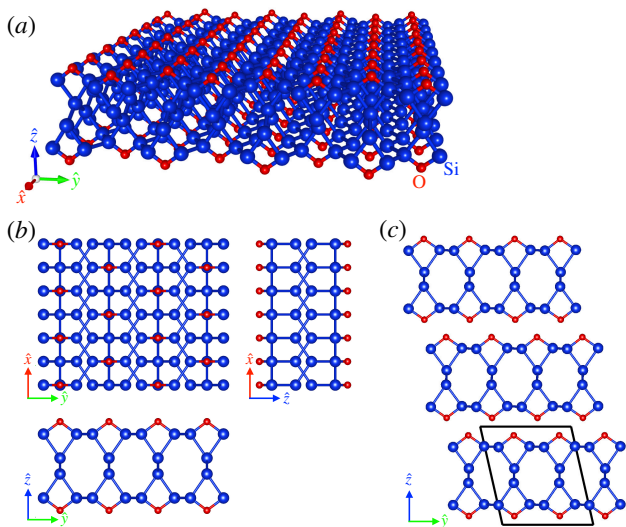


FIG. 1. (a) Schematic atomic configuration of monolayer structure of Si_3O . Red and blue balls denote oxygen and silicon atoms, respectively. (b) Top and side views of the monolayer. (c) The stacking configuration of bulk Si_3O . Black solid lines indicate the unit cell of the layered bulk. Atomic configurations are generated by VESTA [25].

Figures 2(a) and 2(b) show band structures of monolayer and bulk Si_3O , respectively, by using both DFT-PBE and GW_0 calculations. Both systems have direct band gaps (E_g) at the symmetric point of Y. Gaps from other computational methods are summarized in the Table I. Note that the bandgap energies are improved to some extent by using HSE06 functional when compared to the PBE-DFT case, but they are still underestimated by significant amount compared to the quasiparticle bandgaps, indicating self-energy corrections are necessary to investigate optical properties of layered materials. As discussed above, the converged many-body QP gaps can be obtained at the level of the GW_0 approximation. The difference in band gaps (ΔE_g) between DFT-PBE and GW_0 (or self-energy corrections) are 1.35 eV and 0.90 eV for monolayer and bulk, respectively. The different ΔE_g originates from the weaker screening of Coulomb interaction in the monolayer Si_3O than in the bulk. We expect efficient light absorption of Si_3O regardless of the number of layers because both monolayer and bulk Si_3O are direct band gap semiconductors. This is in sharp contrast to MoS_2 which undergoes a direct to indirect band gap transition and a strong photoluminescence of

TABLE I. Direct band gap energies E_g at Y for monolayer and bulk Si_3O calculated by DFT+PBE, hybrid functional HSE06 [41, 42], G_0W_0 and GW_0 approximations.

calculation method	monolayer	bulk
DFT+PBE	0.50 eV	0.35 eV
HSE06 [22]	1.20 eV	1.03 eV
G_0W_0	2.18 eV	1.47 eV
GW_0	1.85 eV	1.25 eV

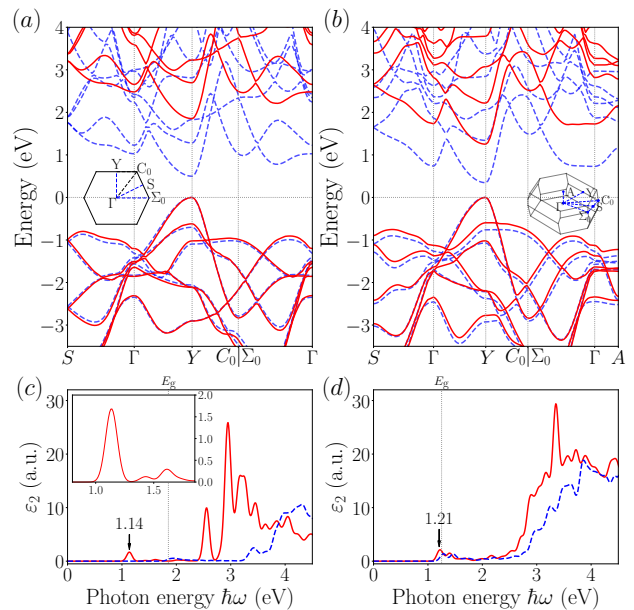


FIG. 2. Energy band structures of (a) monolayer and (b) bulk of Si_3O . Blue dashed and red solid lines represent energy bands calculated from DFT-PBE and GW_0 , respectively. The valence band maximum is set to be zero. Insets show symmetric points in the 1st Brillouin zone. Absorption spectra ϵ_2 of (c) monolayer and (d) bulk from $GW+BSE$ (red solid line) and $GW+RPA$ (blue dashed line). The monolayer spectrum ϵ_2 is normalized by the thickness of the Si_3O relative to the corresponding cell including vacuum padding. The effective thickness of the monolayer is obtained by estimating the distance of two planes parallel to the monolayer Si_3O , between which 99% of the charge density is included. Dotted gray lines indicate photon energy equal to the QP energy gap. The brightest excitons are indicated by black arrows with their energies. The inset in (c) is an enlarged view near 1 eV.

monolayer vanishes when it becomes bilayer or thicker [24]. The robust direct optical absorption regardless of thickness demonstrated in Si_3O here will be very beneficial in PV applications.

We solve the BSE with QP energy bands to investigate optical properties of Si_3O such as frequency-dependent optical absorption spectrum $\epsilon_2(\omega)$ (the imaginary part of the dielectric function) and exciton energy levels. Solving the BSE depends on two calculation parameters: the k -point density and the number of valence and conduction bands for optical transition. We found that $40 \times 40 \times 1$ (monolayer) and $20 \times 20 \times 4$ (bulk) k -point grids and six bands from the valence and conduction band edges suffice to converge $\epsilon_2(\omega)$ up to 4.0 eV. Figures 2(c) and 2(d) show absorption spectra $\epsilon_2(\omega)$ for monolayer and bulk, respectively. The absorption spectra obtained with the electron-hole interaction ($GW+BSE$) are compared with the non-interacting case ($GW+RPA$). We note that the $GW+RPA$ spectra for both monolayer and bulk do not show prominent optical absorption in energy below E_g , marked as the dashed line in Figs. 2(c) and 2(d). Rather, a significant amount of optical absorption appears when the pho-

ton energy exceeds at least about 1.5 eV above E_g . This is due to the energy landscape of the charge carriers over the whole Brillouin zone. As shown in Figs. 2(a) and 2(b), the direct band gap E_g occurs at the Y point, while direct electron-hole pair generation at other momentum would require about 1.5–2.0 eV higher energy than the gap.

When the electron-hole interaction is taken into account, the optical absorption is significantly changed, contrast to the non-interacting case. First, the major absorption peaks are shifted down to the lower photon energy range. This overall red shift of the $GW+BSE$ spectrum with respect to the $GW+RPA$ is more evident in the monolayer than the bulk as shown in Figs. 2(c) and 2(d). As discussed above, a 2D system will have less Coulomb screening along the out-of-plane direction, so its optical absorption can be more strongly affected. Similar to MoS_2 [43], the reduced screening effects in a monolayer limit affect band structures and optical spectra in the opposite way. Monolayer has the larger electronic band gap than bulk (1.85 eV vs 1.25 eV, respectively), but the difference is compensated by the stronger red shift in the absorption spectra (0.8 eV vs 0.2 eV), resulting in almost constant optical band gap of about 1.2 eV regardless of the thickness.

We obtain electron-hole bound states and their energy levels from the BSE. Monolayer shows several optically active exciton states, or bright excitons, below the optical transition continuum in the absorption spectra as shown in Fig. 2(c). The main absorption peak located at 1.14 eV corresponds to the lowest exciton level around Y point with a significant binding energy of 0.72 eV. Other exciton peaks with relatively smaller contributions within the band gap, are depicted in the inset of Fig. 2(c). In contrast, the bulk Si_3O shows a single bright exciton peak at 1.21 eV inside the band gap. The bright exciton at Y is located right below the inter-band transition continuum, implying small binding energy of 40 meV due to the increased screening effect in bulk.

PV efficiency of Si_3O is estimated by calculating the SLME [17] based on the absorption property. The Shockley-Queisser (SQ) limit [44] is an ideal case that photons with energy greater than E_g are perfectly absorbed. However, in reality, light absorption varies with energy according to the absorption coefficient $\alpha(\omega)$. The $\alpha(\omega)$ can be calculated by using the $\epsilon_2(\omega)$ obtained from $GW+BSE$ as follows:

$$\alpha(\omega) = \frac{\omega}{c\tilde{n}(\omega)} \epsilon_2(\omega), \quad (1)$$

where $\tilde{n}(\omega)$ is the real part of the refractive index, $\tilde{n}(\omega) = \sqrt{(\epsilon_1(\omega) + \sqrt{\epsilon_1^2(\omega) + \epsilon_2^2(\omega)})/2}$. Here, real and imaginary parts of the dielectric function, $\epsilon_1(\omega)$ and $\epsilon_2(\omega)$, respectively, are related to each other by the Kramers-Krönig relation [45]. The light absorption is included in the SLME as the absorbance $A(\omega)$, which is given by

$$A(\omega) = 1 - e^{-2\alpha(\omega)L} \quad (2)$$

where L is the material thickness. $A(\omega)$ is derived by assuming both no reflection of a normal incident light at the front

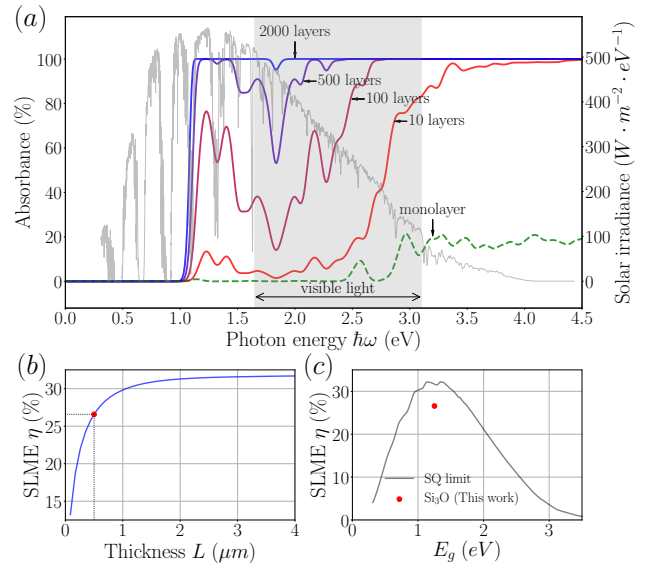


FIG. 3. (a) Absorbance spectra from $GW+BSE$ for monolayer and bulk Si_3O of 10, 100, 500, and 2000 layers whose thicknesses in μm are 8.208×10^{-4} , 8.695×10^{-3} , 8.695×10^{-2} , 0.435, and 1.739, respectively. The gray box indicates the energy range of visible light. The AM1.5 is shown with gray lines. (b) The SLME (η) as a function of thickness L at 25°C. (c) η at $L = 0.5 \mu m$ is shown together with the SQ limit curve as a function of the band gap.

surface and perfect reflection at the back surface of the photovoltaic material [17]. Due to the unity reflection [17], the net distance traveled by light within the material is $2L$.

Figure 3(a) shows calculated absorbance spectra for monolayer and bulk Si_3O with different thicknesses. The absorbance $A(\omega)$ in Eq. (2) increases with the L because there is an increasing chance to be absorbed when light travels further inside the material. We note, however, that the monolayer Si_3O can demonstrate desirable optoelectronic properties for particular applications; it shows a great sunlight absorption ranging 10–22 % in the visible range, which is comparable to monolayer MoS_2 (about 10–20 % with unity reflection at the back surface) [46], and extremely light effective masses for both electrons and holes ($\sim 0.03 m_0$ with m_0 being an electron rest mass) as shown in Fig. S3 in the ESI, indicating its good transport properties. All in all, the monolayer Si_3O is promising for a semitransparent solar cell or flexible transparent conducting electrode. Furthermore, contrast to other 2D materials (e.g., MoS_2), the electronic structures show direct optical transitions regardless of the number of layers, which enables the Si_3O to be directly used as a macroscopic active layer in PV devices.

When the film is very thin (10 layers), the absorbance spectrum [Fig. 3(a)] looks similar to the absorption spectrum shown in Fig. 2(d). For 100 layers, the absorbance in the high energy regime (> 2.7 eV) becomes saturated to be unity. In contrast to the 10 layer case, drastically enhanced absorbance is shown even in the low energy range from E_g to about 2.5

eV due to the increased thickness. In particular, two dominant peaks below 1.5 eV reaches about 60 %. As thickness further increases, the absorbance approaches to unity in the wider range of energy. The absorbance in the vicinity of 1.8 eV, which corresponds to the absorption coefficient minimum, increases relatively slowly, but it finally approaches to unity when bulk Si₃O is thick enough.

We also calculate the SLME as a function of thickness to investigate how the absorbance affects the PV efficiency. Given the total incident solar energy density P_{in} based on the Air Mass 1.5 data [47], the SLME of $\eta = \max[P]/P_{in}$ is obtained by maximizing the output power density $P = JV$, the product of the net current density J and voltage V [17]. Figure 3(b) shows that the SLME reaches 30.4% at thickness of about 1.8 μm , comparable to the SQ limit of 31.67%. In case of $L = 0.5 \mu\text{m}$ and the temperature $T = 25^\circ\text{C}$, the standard thickness for comparisons [17, 18], the SLME is about 26.81%, which is shown on top of the SQ limit in Fig. 3(c).

In conclusion, we have shown that the layered Si₃O has a favorable optical gap for solar light absorption that is nearly independent of the number of layers. Its computed PV efficiency is also comparable to the ideal limit. Thus, we believe that the new two-dimensional silicon oxide suggested here possesses highly desirable characteristics for solar cell, composed of a single element and oxygen which is quite analogous to the currently dominant solar cell material.

CONFLICTS OF INTEREST

There are no conflicts of interest to declare.

ACKNOWLEDGEMENT

S. K. was supported by the KISTI National Supercomputing Center with supercomputing resources including technical support (KSC-2019-CRE-0040) and by the Open KIAS Center at Korea Institute for Advanced Study. Y.-W.S. was supported by the NRF of Korea (Grant No. 2017R1A5A1014862, SRC program: vdWMRC Center) and by KIAS individual grant (CG031509).

* corresponding author: kisung@kias.re.kr

† corresponding author: hand@kias.re.kr

- [1] N. M. Haegel, R. Margolis, T. Buonassisi, D. Feldman, A. Froitzheim, R. Garabedian, M. Green, S. Glunz, H.-M. Henning, B. Holder, I. Kaizuka, B. Kroposki, K. Matsubara, S. Niki, K. Sakurai, R. A. Schindler, W. Tumas, E. R. Weber, G. Wilson, M. Woodhouse, and S. Kurtz, *Science* **356**, 141 (2017).
- [2] Q. H. Wang, K. Kalantar-Zadeh, A. Kis, J. N. Coleman, and M. S. Strano, *Nat. Nano.* **7**, 699 (2012).
- [3] A. C. Ferrari, F. Bonaccorso, V. Fal'ko, K. S. Novoselov, S. Roche, P. Bøggild, S. Borini, F. H. L. Koppens, V. Palermo, N. Pugno, J. A. Garrido, R. Sordan, A. Bianco, L. Ballerini, M. Prato, E. Lidorikis, J. Kivioja, C. Marinelli, T. Ryhänen, A. Morpurgo, J. N. Coleman, V. Nicolosi, L. Colombo, A. Fert, M. Garcia-Hernandez, A. Bachtold, G. F. Schneider, F. Guinea, C. Dekker, M. Barbone, Z. Sun, C. Galiotis, A. N. Grigorenko, G. Konstantatos, A. Kis, M. Katsnelson, L. Vandersypen, A. Loiseau, V. Morandi, D. Neumaier, E. Treossi, V. Pellegrini, M. Polini, A. Tredicucci, G. M. Williams, B. Hee Hong, J.-H. Ahn, J. Min Kim, H. Zirath, B. J. van Wees, H. van der Zant, L. Occhipinti, A. Di Matteo, I. A. Kinloch, T. Seyller, E. Quesnel, X. Feng, K. Teo, N. Rupesinghe, P. Hakonen, S. R. T. Neil, Q. Tannock, T. Löfwander, and J. Kinaret, *Nanoscale* **7**, 4598 (2015).
- [4] F. Bonaccorso, L. Colombo, G. Yu, M. Stoller, V. Tozzini, A. C. Ferrari, R. S. Ruoff, and V. Pellegrini, *Science* **347**, 1246501 (2015).
- [5] K. S. Novoselov, A. Mishchenko, A. Carvalho, and A. H. Castro Neto, *Science* **353**, aac9439 (2016).
- [6] D. Jariwala, A. R. Davoyan, J. Wong, and H. A. Atwater, *ACS Photonics* **4**, 2962 (2017).
- [7] S. Das, D. Pandey, J. Thomas, and T. Roy, *Adv. Mat.* **31**, 1802722 (2019).
- [8] M. Ashton, J. Paul, S. B. Sinnott, and R. G. Hennig, *Phys. Rev. Lett.* **118**, 106101 (2017).
- [9] N. Mounet, M. Gibertini, P. Schwaller, D. Campi, A. Merkys, A. Marrazzo, T. Sohier, I. E. Castelli, A. Cepellotti, G. Pizzi, and N. Marzari, *Nature Nanotechnology* **13**, 246 (2018).
- [10] T. S. Bush, C. R. A. Catlow, and P. D. Battle, *J. Mater. Chem.* **5**, 1269 (1995).
- [11] A. R. Oganov and C. W. Glass, *J. Chem. Phys.* **124**, 244704 (2006).
- [12] Y. Wang, J. Lv, L. Zhu, and Y. Ma, *Phys. Rev. B* **82**, 094116 (2010).
- [13] D. Y. Kim, S. Stefanoski, O. O. Kurakevych, and T. A. Strobel, *Nature Materials* **14**, 169 (2015).
- [14] D. Davies, K. T. Butler, J. M. Skelton, C. Xie, A. R. Oganov, and A. Walsh, *Chem. Sci.* **9**, 1022 (2018).
- [15] T. Gu, W. Luo, and H. Xiang, *WIREs Comput Mol Sci* **7** (2017), 10.1002/wcms.1295.
- [16] O. Kononova, H. Huo, T. He, Z. Rong, T. Botari, W. Sun, V. Tshitoyan, and G. Ceder, *Phys. Rev. Lett.* **108**, 068701 (2012).
- [17] L. Yu and A. Zunger, *Phys. Rev. Lett.* **108**, 068701 (2012).
- [18] K. Choudhary, M. Bercx, J. Jiang, R. Pachter, D. Lamoen, and F. Tavazza, *Chemistry of Materials* **31**, 5900 (2019).
- [19] Q. Wang, J. Li, Y. Liang, Y. Nie, and B. Wang, *ACS Appl. Mater. Interfaces* **10**, 41670 (2018).
- [20] H. Yang, Y. Ma, Y. Liang, B. Huang, and Y. Dai, *ACS Appl. Mater. Interfaces* **11**, 37901 (2019).
- [21] P. Zhao, H. Yang, J. Li, H. Jin, W. Wei, L. Yu, B. Huang, and Y. Dai, *J. Mater. Chem. A* **5**, 24145 (2017).
- [22] K. Chae and Y.-W. Son, *Nano. Lett.* **19**, 2694 (2019).
- [23] K. Chae, D. Y. Kim, and Y.-W. Son, *2D Mater.* **5**, 025013 (2018).
- [24] K. F. Mak, C. Lee, J. Hone, J. Shan, and T. F. Heinz, *Phys. Rev. Lett.* **105**, 136805 (2010).
- [25] K. Momma and F. Izumi, *Commission on Crystallogr. Comput., IUCr Newsl.* **7**, 106 (2006).
- [26] J. P. Perdew, K. Burke, and M. Ernzerhof, *Phys. Rev. Lett.* **77**, 3865 (1996).
- [27] P. Giannozzi, O. Andreussi, T. Brumme, O. Bunau, M. B. Nardelli, M. Calandra, R. Car, C. Cavazzoni, D. Ceresoli, M. Cococcioni, N. Colonna, I. Carnimeo, A. D. Corso, S. de Gironcoli, P. Delugas, R. A. D. Jr, A. Ferretti, A. Floris, G. Fratesi, G. Fugallo, R. Gebauer, U. Gerstmann, F. Giustino, T. Gorni, J. Jia, M. Kawamura, H.-Y. Ko, A. Kokalj, E. Küçük-

- benli, M. Lazzeri, M. Marsili, N. Marzari, F. Mauri, N. L. Nguyen, H.-V. Nguyen, A. O. de-la Roza, L. Paulatto, S. Ponc e, D. Rocca, R. Sabatini, B. Santra, M. Schlipf, A. P. Seitsonen, A. Smogunov, I. Timrov, T. Thonhauser, P. Umari, N. Vast, X. Wu, and S. Baroni, *J. Phys.: Condens. Matter* **21**, 395502 (2009).
- [28] P. Giannozzi, S. Baroni, N. Bonini, M. Calandra, R. Car, C. Cavazzoni, D. Ceresoli, G. L. Chiarotti, M. Cococcioni, I. D. and A. Dal Corso, S. Fabris, G. Fratesi, S. de Gironcoli, R. Gebauer, U. Gerstmann, C. Gougoussis, A. Kokalj, M. Lazzeri, L. Martin-Samos, N. Marzari, F. Mauri, R. Mazzarelli, S. Paolini, A. Pasquarello, L. Paulatto, C. Sbraccia, S. Scandolo, G. Sciauzero, A. P. Seitsonen, A. Smogunov, P. Umari, and R. M. Wentzcovitch, *J. Phys.: Condens. Matter* **29**, 465901 (2017).
- [29] S. Grimme, *J. Comp. Chem.* **27**, 1787 (2006).
- [30] L. Hedin, *Phys. Rev.* **139**, A796 (1965).
- [31] J. Deslippe, G. Samsonidze, M. Jain, M. L. Cohen, and S. G. Louie, *Phys. Rev. B* **87**, 165124 (2013).
- [32] E. E. Salpeter and H. A. Bethe, *Phys. Rev.* **84**, 1232 (1951).
- [33] S. Albrecht, L. Reining, R. D. Sole, and G. Onida, *Phys. Rev. Lett.* **80**, 4510 (1998).
- [34] L. X. Benedict, E. L. Shirley, and R. B. Bohn, *Phys. Rev. Lett.* **80**, 4514 (1998).
- [35] M. Hybertsen and S. Louie, *Phys. Rev. B* **34**, 5390 (1986).
- [36] M. Rohlfing and S. G. Louie, *Phys. Rev. Lett.* **81**, 2312 (1998).
- [37] M. Rohlfing and S. G. Louie, *Phys. Rev. B* **62**, 4927 (2000).
- [38] J. Deslippe, G. Samsonidze, D. A. Strubbe, M. Jain, M. L. Cohen, and S. G. Louie, *Comput. Phys. Commun.* **183**, 1269 (2012).
- [39] S. Ismail-Beigi, *Phys. Rev. B* **73**, 233103 (2006).
- [40] D. Y. Qiu, F. H. da Jornada, and S. G. Louie, *Phys. Rev. Lett.* **111**, 216805 (2013).
- [41] J. Heyd, G. E. Scuseria, and M. Ernzerhof, *J. Chem. Phys.* **118**, 8207 (2003).
- [42] A. V. Krugau, O. A. Vydrov, A. F. Izmaylov, and G. E. Scuseria, *J. Chem. Phys.* **125**, 224106 (2006).
- [43] D. Y. Qiu, F. H. da Jornada, and S. G. Louie, *Phys. Rev. B* **93**, 235435 (2016).
- [44] W. Shockley and H. J. Queisser, *J. Appl. Phys.* **32**, 510 (1961).
- [45] M. P. Marder, *Condensed Matter Physics*, 2nd ed. (John Wiley & Sons, Inc., 2010).
- [46] M. Bernardi, M. Palummo, and J. C. Grossman, *Nano Lett.* **13**, 3664 (2013).
- [47] "Reference solar spectral irradiance: Air mass 1.5," <https://rredc.nrel.gov/solar//spectra/am1.5/>.

Electronic Supplementary Information for: "Promising photovoltaic efficiency of a layered silicon oxide crystal Si₃O"

Sejoong Kim,^{1,2} Kisung Chae,^{2,3,4,*} and Young-Woo Son^{2,†}

¹ *University of Science and Technology (UST), Daejeon 34113, Korea*

² *Korea Institute for Advanced Study, Seoul 02455, Korea*

³ *Department of Chemistry and Biochemistry, University of California, San Diego, La Jolla, CA 92093, United States*

⁴ *Materials Science and Engineering Department, The University of Texas at Dallas, Richardson, Texas 75080, United States*

(Dated: August 7, 2020)

COMPUTATIONAL DETAILS

We perform the DFT calculations in order to construct mean-field wavefunctions and energy bands for the GW calculations. We use the QUANTUM ESPRESSO [S1, S2] with the plane-wave basis, the PBE exchange-correlation functional [S3] and norm-conserving pseudopotentials [S4, S5]. For the self-consistent calculation, $24 \times 24 \times 1$ and $24 \times 24 \times 4$ k -point grids are adopted for monolayer and bulk respectively. Energy cutoff 952 eV is used for the plane wave expansion. We use the semiempirical Grimme's DFT-D2 scheme [S6] for the van der Waal's correction in order to obtain the fully relaxed structure of the layered bulk Si₃O.

The GW calculations are performed by using the BERKELEYGW package [S7] at the level of G_0W_0 and GW_0 . Electronic self-energy is calculated by using the generalized plasmon-pole model [S8] and the modified static remainder approach [S9]. The convergence of the quasi-particle (QP) band structure are achieved by tuning parameters such as the k -point grid, the energy cutoff of the dielectric matrix $\epsilon_{\mathbf{G},\mathbf{G}'}^{-1}$, and the number of unoccupied bands N_b . The Coulomb interaction truncation scheme [S10] is used to simulate the isolated monolayer geometry of Si₃O. Considering that the QP band structure for low-dimensional systems can show a very slow convergence as a function of the size of the vacuum region as reported in Ref. S11, the convergence of the QP band structure is also checked by varying the size of vacuum. The parameters mentioned above are tuned in order to converge the QP energy gap within 50 meV.

We use the energy cutoff 340 eV for the dielectric matrix $\epsilon_{\mathbf{G},\mathbf{G}'}^{-1}$, and $N_b = 1000$ unoccupied bands for mono-layer and bulk of Si₃O. Figure S1 shows the convergence behavior of the QP band gap at the symmetric point Y as a function of the number of unoccupied bands N_b and the energy cutoff of the dielectric function $\epsilon_{\mathbf{G},\mathbf{G}'}^{-1}$. In our calculation $14 \times 14 \times 1$ and $6 \times 6 \times 3$ k -grids are sampled for monolayer and bulk, respectively. We increase the cell size up to 40 Å along the normal direction to the layer plane.

Self-consistently iterative calculations on G are performed to calculate QP band gaps in the so-called GW_0 approximation. It is shown that the corresponding band gaps determined by GW_0 approximation are converged to the QP band gap linearly

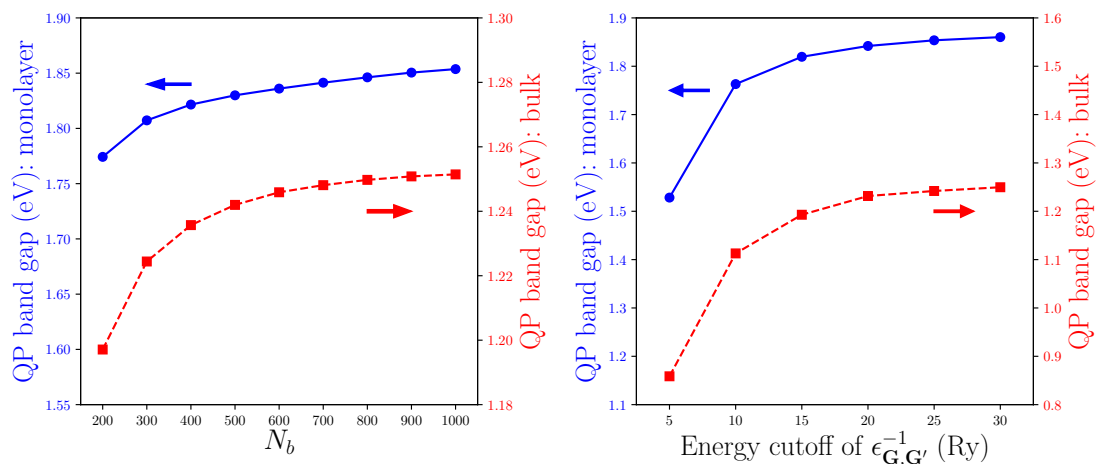


FIG. S1. (Color online) Convergence behaviors of QP band gaps as a function of (a) the number of unoccupied bands N_b and (b) the energy cutoff of the dielectric function $\epsilon_{\mathbf{G},\mathbf{G}'}^{-1}$. QP band gaps of monolayer and bulk Si₃O are indicated by blue solid lines and red dashed lines, respectively.

interpolated from the G_0W_0 gap [S8]. Within three iterations the difference between the G_3W_0 gap and the linearly interpolated gap becomes smaller than 5 meV.

We solve the Bethe-Salpeter equation (BSE) with QP energy bands of Si_3O in order to obtain optical absorption spectrum $\epsilon_2(\omega)$ (the imaginary part of the dielectric function) and exciton energy levels. The numerical solution of the BSE depends on the size of k -point mesh and the number of valence and conduction bands. $40 \times 40 \times 1$ and $20 \times 20 \times 4$ k -point grids are used to reproduce well-converged absorption spectra for monolayer and bulk Si_3O , respectively. In our calculation six highest valence bands and six lowest conduction ones are used to solve the BSE, and it is shown that the absorption spectrum is well converged up to about 4.0 eV. Gaussian broadening of 0.05 eV is adopted to numerically calculate the absorption spectrum. The absorption spectrum is calculated on the energy grid whose interval is $\hbar\Delta\omega = 0.01$, on which the numerical integration is performed for the spectroscopic limited maximum efficiency (SLME) [S12].

The analytic expression of the absorption spectrum $\epsilon_2(\omega)$ involves the delta function, which can be replaced by the Gaussian function with the broadening parameter in the numerical calculation. The broadening parameter, which is in principle small, is needed to be a finite value suitable to numerical integrations for $\epsilon_2(\omega)$ and the SLME η , which are based on the \mathbf{k} -point mesh and the discrete grid of ω . If the broadening parameter is smaller than the energy resolution of the integration, the spectrum $\epsilon_2(\omega)$ shows spurious and bumpy features due to the finite sampling. In contrast, too large smearing parameter can wash out important detailed features of the spectrum. We have tested the effect of broadening parameters for $\epsilon_2(\omega)$ on SLME calculations. The calculations show that the SLME η maintains about 26–27% within the range from 0.02 to 0.06. If the smearing parameter is smaller than the energy resolution $\hbar\Delta\omega = 0.01$ eV, or it is much larger (> 0.08 eV), the SLME η deviates from 26–27% as shown in Fig S2(b).

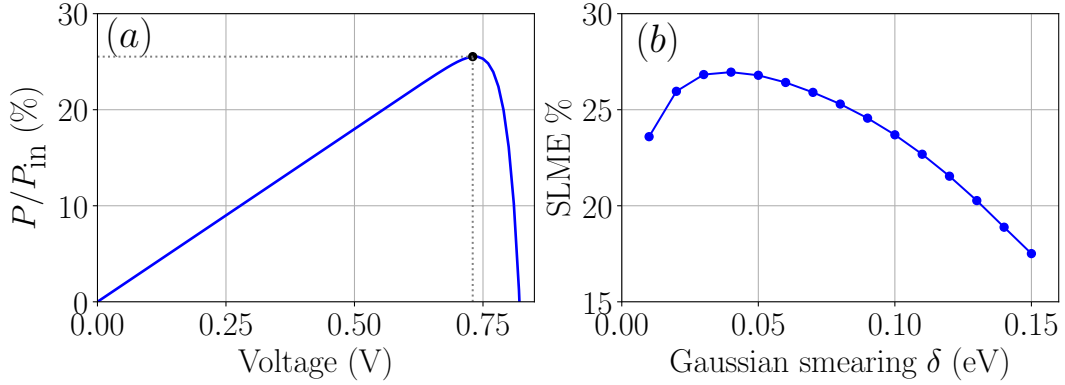


FIG. S2. (Color online) (a) P/P_{in} (blue solid line) as a function of the voltage V . The SLME η , the maximum value of P/P_{in} , is indicated by black circle. (b) SLME η calculations by tuning the broadening parameter from 0.01 to 0.15.

SLME CALCULATIONS

The SLME η of the solar cell can be calculated by maximizing the ratio P/P_{in} [S12, S13]. Here the total incident solar energy density P_{in} is calculated by using the Air Mass 1.5 data [S14] for the solar irradiance spectrum of the photon flux $I_{AM1.5}(E)$,

$$P_{in} = \int_0^{\infty} I_{AM1.5}(E) E dE. \quad (3)$$

The output power density of the solar cell P is the product of the total net current density J and the voltage V ,

$$P = JV = \left[J_{sc} - J_0 \left(e^{eV/k_B T} - 1 \right) \right] V, \quad (4)$$

where e , k_B , and T are the electron charge, the Boltzmann constant, and the solar cell temperature, respectively [S12, S13]. The net current density J is determined by two contributions: the short-circuit current density J_{sc} and the reverse saturation current density J_0 . The short-circuit current density J_{sc} is calculated from the absorbance $A(E)$ and the AM1.5 spectrum $I_{AM1.5}(E)$,

$$J_{sc} = e \int_0^{\infty} A(E) I_{AM1.5}(E) dE. \quad (5)$$

J_0 is further expressed as the sum of the non-radiative electron-hole combination current density J_0^{nr} and the radiative one J_0^r ,

$$J_0 = J_0^{nr} + J_0^r = \frac{J_0^r}{f_r}. \quad (6)$$

Here $f_r = J_0^r / (J_0^{nr} + J_0^r)$ is the fraction of the radiative combination current, which is approximately given by $f_r = e^{-(E_g^{da} - E_g)/k_B T}$, where E_g and E_g^{da} are the minimum gap and the directly allowed gap, respectively [S12, S13]. Considering the principle of the detailed balance, the radiative combination current J_0^r is equal to the absorption rate of photons from the surrounding thermal path in equilibrium with the solar cell surface:

$$J_0^r = e\pi \int_0^\infty A(E) I_{bb}(E, T) dE, \quad (7)$$

where $I_{bb}(E, T)$ stands for the spectrum of the black body at temperature T ,

$$I_{bb}(E, T) = \frac{2\pi}{h^3 c^2} \frac{E^2}{e^{E/k_B T} - 1}, \quad (8)$$

where h and c are the Planck constant and the speed of light, and the temperature of the surrounding thermal bath is $T = 25^\circ\text{C}$ in this work. The SLME η can be obtained by numerically maximizing P as shown in Fig. S2(a).

THERMAL STABILITY OF Si₃O

Here, *ab initio* molecular dynamics (AIMD) is employed to show robust thermal stability of Si₃O in addition to convex Hull and harmonic phonon dispersion provided in Ref. S15. The Si₃O monolayer is expanded to a (3×3×1) supercell which contains 18 Si₃O formula units. AIMD is performed at a temperature of 1,500 K in canonical ensemble (i.e., constant NVT), where temperature of the system is controlled by Nosé-Hoover thermostat. The system is integrated by using Verlet algorithm for 10 pico seconds (or 10,000 steps) with a time step of 1 femto second. Fig. S3 shows temporal evolution of energy and temperature of the system during the AIMD calculation. The instantaneous energy seems to fluctuate around a constant value within a reasonable energy window, indicating that the temporal average is kept constant. This means that the atomic arrangements in the Si₃O remain stable without any broken bonds throughout the AIMD calculations. The inset in Fig. S3 shows a snapshot of the Si₃O monolayer during the AIMD. Each of the atoms vibrates at their equilibrium positions due to the kinetic energy, but the initial structure is maintained, confirming the robust thermal stability.

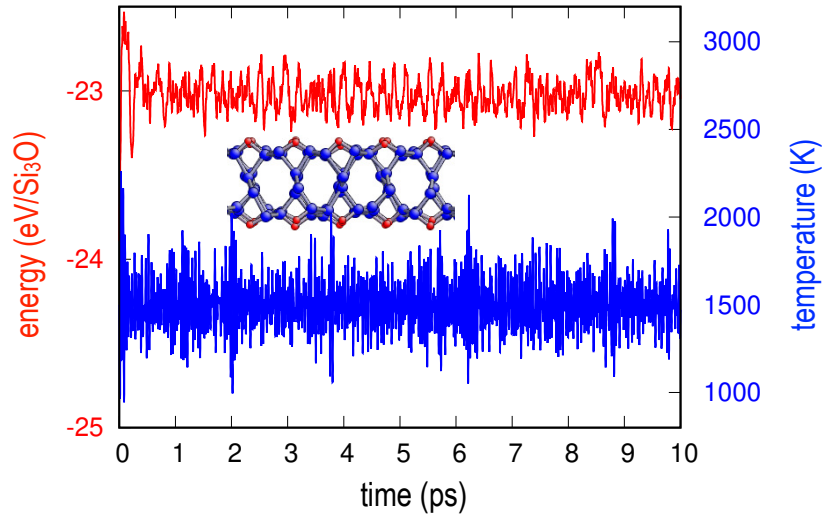


FIG. S3. (Color online) Evolution of energy (red) and temperature (blue) with elapsed time. Snapshot of Si₃O is shown in the inset.

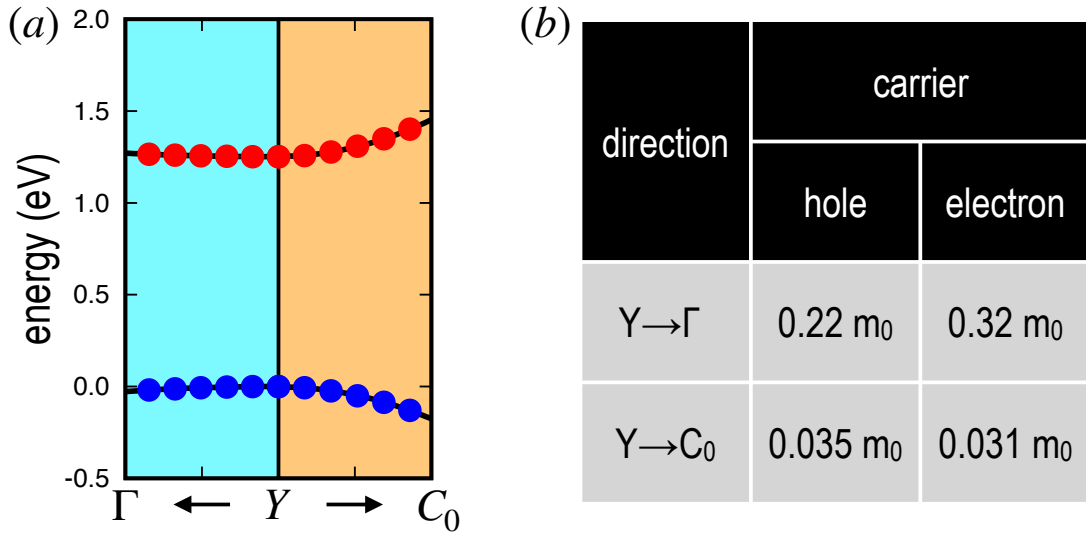


FIG. S4. (Color online) Effective masses of Si_3O . (a) Quasiparticle eigenvalues near the band edges: conduction (red symbols) and valence (blue symbols) bands along Y - Γ (cyan shading) and Y - C_0 (orange shading) directions. The black curves behind the data points are fitted to quadratic functions. (b) The calculated effective masses are tabulated relative to an electron rest mass m_0 .

EFFECTIVE MASSES IN Si_3O

Carrier mobility (μ) is an important characteristic in photovoltaic applications for efficient charge separation and photo-current collection. In solids, the carrier mobility can be shown as

$$\mu = \frac{q\tau}{2m^*}$$

where q is an elemental charge, τ is scattering time and m^* is an effective mass. The scattering time τ depends on various factors such as details of electronic structures, defect concentrations and temperature, and electron-phonon scattering becomes a dominant factor for pure bulk materials with few defects. While elaborated evaluation of the τ is crucial for the quantitative assessment of carrier mobility, it will require demanding computation of electron-phonon coupling matrix, which is beyond the scope of this paper. As a crude approximation, we hypothesize that effective masses (m^*) be sufficient to possibly show qualitative picture of carrier mobility behaviors in Si_3O . We investigate the in-plane effective masses in bulk Si_3O from quasiparticle band structures as shown in Fig. 2(b). Two high-symmetry paths are considered: from Y to Γ and from Y to C_0 , and small fractions of each path around the Y momentum, where both maximum and minimum occur, are shown in Fig. S4(a). Quasiparticle eigenvalues along each of the paths in each band are used to separately fit the harmonic energy-momentum (E - k) dispersion behavior near the band edges, i.e.,

$$E(k) = E_0 + \frac{\hbar k^2}{2m^*}$$

where \hbar is Planck constant. The effective mass can be obtained from the curvature of the second derivative of the band structure,

$$(m^*)^{-1} = \frac{1}{\hbar} \frac{d^2 E}{dk^2}$$

which is usually used relative to the electron rest mass m_0 . Figure S4(b) shows the m^* for each direction and for both electron and hole. It is interesting that the effective masses for both electron and hole along different directions show an order-of-magnitude difference, indicating that the Si_3O is highly anisotropic. Moreover, the effective mass values of the *light* bands for both electron and hole are remarkably small ($\sim 0.03 m_0$), comparable to well-known high mobility semiconductors such as InSb ($0.0135 m_0$) and GaAs ($0.067 m_0$) [S16]. Even for the *heavy* bands, the effective mass values are comparable to a bulk silicon crystal ($0.19 m_0$ and $0.16 m_0$ for electron and hole, respectively). It is worth noting that the band edges at Y serve as the sole predominant inter-band transition path across the band gap up to a few hundreds meV, limiting the number of possible electron-phonon coupling pathways up to considerable temperature range. With remarkably small effective masses for both electron and hole as well as

the interesting electronic structures favorable for efficient carrier transport, Si_3O makes a promising candidate for photovoltaic applications.

* corresponding author: kisung@kias.re.kr

† corresponding author: hand@kias.re.kr

- [S1] P. Giannozzi, O. Andreussi, T. Brumme, O. Bunau, M. Buongiorno Nardelli, M. Calandra, R. Car, C. Cavazzoni, D. Ceresoli, M. Cococcioni, N. Colonna, I. Carnimeo, A. Dal Corso, S. de Gironcoli, P. Delugas, R. A. DiStasio Jr, A. Ferretti, A. Floris, G. Fratesi, G. Fugallo, R. Gebauer, U. Gerstmann, F. Giustino, T. Gorni, J. Jia, M. Kawamura, H.-Y. Ko, A. Kokalj, E. Küçükbenli, M. Lazzeri, M. Marsili, N. Marzari, F. Mauri, N. L. Nguyen, H.-V. Nguyen, A. Otero de-la Roza, L. Paulatto, S. Poncè, D. Rocca, R. Sabatini, B. Santra, M. Schlipf, A. P. Seitsonen, A. Smogunov, I. Timrov, T. Thonhauser, P. Umari, N. Vast, X. Wu, and S. Baroni, *J. Phys.: Condens. Matter* **21**, 395502 (2009).
- [S2] P. Giannozzi, S. Baroni, N. Bonini, M. Calandra, R. Car, C. Cavazzoni, D. Ceresoli, G. L. Chiarotti, M. Cococcioni, I. Dabo and A. Dal Corso, S. Fabris, G. Fratesi, S. de Gironcoli, R. Gebauer, U. Gerstmann, C. Gougoussis, A. Kokalj, M. Lazzeri, L. Martin-Samos, N. Marzari, F. Mauri, R. Mazzarello, S. Paolini, A. Pasquarello, L. Paulatto, C. Sbraccia, S. Scandolo, G. Sclauzero, A. P. Seitsonen, A. Smogunov, P. Umari, and R. M. Wentzcovitch, *J. Phys.: Condens. Matter* **29**, 465901 (2017).
- [S3] J. P. Perdew, K. Burke, and M. Ernzerhof, “Generalized gradient approximation made simple,” *Phys. Rev. Lett.* **77**, 3865 (1996).
- [S4] D. Hamann, M. Schlüter, and C. Chiang, “Norm-conserving pseudopotentials,” *Phys. Rev. Lett.* **43**, 1494–1497 (1979).
- [S5] G. Bachelet, D. Hamann, and M. Schlüter, “Pseudopotentials that work: From h to pu,” *Phys. Rev. B* **26**, 4199–4228 (1982).
- [S6] S. Grimme, “Semiempirical gga-type density functional constructed with a long-range dispersion correction,” *J. Comp. Chem.* **27**, 1787 (2006).
- [S7] J. Deslippe, G. Samsonidze, D. A. Strubbe, M. Jain, M. L. Cohen, and S. G. Louie, “Berkeleygw: A massively parallel computer package for the calculation of the quasiparticle and optical properties of materials and nanostructures,” *Comput. Phys. Commun.* **183**, 1269 (2012).
- [S8] M. Hybertsen and S. Louie, “Electron correlation in semiconductors and insulators: Band gaps and quasiparticle energies,” *Phys. Rev. B* **34**, 5390–5413 (1986).
- [S9] J. Deslippe, G. Samsonidze, M. Jain, M. L. Cohen, and S. G. Louie, “Coulomb-hole summations and energies for gw calculations with limited number of empty orbitals: A modified static remainder approach,” *Phys. Rev. B* **87**, 165124 (2013).
- [S10] S. Ismail-Beigi, “Truncation of periodic image interactions for confined systems,” *Phys. Rev. B* **73**, 233103 (2006).
- [S11] D. Y. Qiu, F. H. da Jornada, and S. G. Louie, “Optical spectrum of MoS_2 : Many-body effects and diversity of excitation states,” *Phys. Rev. Lett.* **111**, 216805 (2013).
- [S12] L. Yu and A. Zunger, “Identification of potential photovoltaic absorbers based on first-principles spectroscopic screening of materials,” *Phys. Rev. Lett.* **108**, 068701 (2012).
- [S13] Kamal Choudhary, Marnik Bercx, Jie Jiang, Ruth Pachter, Dirk Lamoen, and Francesca Tavazza, “Accelerated discovery of efficient solar cell materials using quantum and machine-learning methods,” *Chemistry of Materials* **31**, 5900–5908 (2019).
- [S14] “Reference solar spectral irradiance: Air mass 1.5,” <https://rredc.nrel.gov/solar//spectra/am1.5/>.
- [S15] Kisung Chae and Young-Woo Son, “A new family of two-dimensional crystals: Open-framework T_3X ($\text{T} = \text{C}, \text{Si}, \text{Ge}, \text{Sn}$; $\text{X} = \text{O}, \text{S}, \text{Se}, \text{Te}$) compounds with tetrahedral bonding,” *Nano. Lett.* **19**, 2694–2699 (2019).
- [S16] I. Vurgaftman, J. R. Meyer, and L. R. Ram-Mohan, “Band parameters for iii–v compound semiconductors and their alloys,” *Journal of Applied Physics* **89**, 5815–5875 (2001).